Progress In Electromagnetics Research, Vol. 107, 331–348, 2010

DATA INDEPENDENT RADAR BEAMFORMING ALGORITHMS FOR BREAST CANCER DETECTION

D. Byrne, M. O'Halloran, M. Glavin, and E. Jones †

College of Engineering and Informatics
National University of Ireland Galway
University Road, Galway, Ireland

Abstract—Ultra wideband (UWB) Microwave imaging is one of the most promising emerging imaging technologies for breast cancer detection, and is based on the dielectric contrast between normal and cancerous tissues at microwave frequencies. UWB radar imaging involves illuminating the breast with a microwave pulse and reflected signals are used to determine the presence and location of significant dielectric scatterers, which may be representative of cancerous tissue within the breast. Beamformers are used to spatially focus the reflected signals and to compensate for path dependent attenuation and phase effects. While these beamforming algorithms have often been evaluated in isolation, variations in experimental conditions and metrics prompts the assessment of the beamformers on common anatomically and dielectrically representative breast models in order to effectively compare the performance of each. This paper seeks to investigate the following beamforming algorithms: Monostatic and Multistatic Delay-And-Sum (DAS), Delay-Multiply-And-Sum (DMAS) and Improved Delay-And-Sum (IDAS). The performance of each beamformer is evaluated across a range of appropriate metrics.

1. INTRODUCTION

In 2009, there were approximately 1.5 million new cases of breast cancer documented in the US alone [1], while the estimated mortality rate in Europe was over 1.7 million [2]. The current *de facto* breast cancer screening method is X-Ray mammography, and despite

Received 10 June 2010, Accepted 30 June 2010, Scheduled 17 August 2010
Corresponding author: D. Byrne (dallanbyrne@gmail.com).
† All are also with Bioelectronics Research Cluster, National Centre for Biomedical Engineering Science (NCBES), National University of Ireland Galway, University Road, Galway, Ireland.

success in detecting early stage breast cancer, there are a number of well documented limitations with the technology [3, 4]. MRI offers improved image quality compared to X-Ray and although non-ionizing and non-invasive, high operating costs make it unsuitable for mass screening. Ultrasound imaging, although less expensive, is limited by resolution and issues of speckle in the resultant images. Such limitations have prompted the investigation of improved breast imaging technologies, in order to accurately diagnose breast cancer at minimum risk and discomfort to the patient.

One such promising modality is microwave breast imaging, which uses backscattered radar signals to identify cancerous tissue within the breast. Microwave imaging of the breast can be categorized by three distinct approaches: UWB radar imaging [5–10], Microwave Tomography [11, 12] and Hybrid imaging techniques [13, 14]. Microwave Tomography attempts to reconstruct the entire dielectric profile of the breast from the solution of an inverse scattering problem. Hybrid techniques like Microwave-Induced Thermoacoustic Tomography [13] is based on the principle that electromagnetic (EM) energy absorbed by malignant tissue will induce sonic reverberations, which can be detected by a transducer.

Finally, UWB radar imaging involves illuminating the breast with a sub-nanosecond microwave pulse. The dielectric contrast between tissue types, notably malignant and normal breast tissues, generate EM reflections within the breast. These reflections are recorded and a time-domain image-formation algorithm (beamformer) is applied to determine the spatial location of any dielectric scatterer present. Data-Independent (DI) beamformers use an assumed propagation model to compensate for path dependent attenuation and dispersion [5–8].

Several factors make it difficult to directly compare the performance of beamforming algorithms:

- The use of very different numerical breast phantoms, with 2D and 3D beamformer evaluations [7, 8, 15, 16] and significant variations in the level of modeled heterogeneity [17–20].
- The use of different radar configurations (Monostatic [6, 7] and Multistatic [10, 15]).
- Variations in antenna array geometry [21].

This paper attempts to examine the performance of several DI beamforming algorithms using common anatomically-accurate breast models. The paper is organized as follows: Section 2 details the various DI beamforming algorithm, while the numerical breast model model is documented in Section 3. Performance metrics are described in Section 4 and results are presented and discussed in Section 5. Concluding remarks are outlined in the final section.

2. DATA-INDEPENDENT METHODS

A DI beamformer uses an assumed propagation model to approximate a desired response independent of the input signal data. Most DI beamforming algorithms are based on a classical broadband beamformer, where the algorithm approximates the propagation delays of the signals in order to focus the combined response at a specific location. In this section a detailed description of the Monostatic and Multistatic Delay-And-Sum (DAS), Delay-Multiply-And-Sum (DMAS) and Improved-Delay-And-Sum (IDAS) beamformers is presented. DMAS and IDAS are Multistatic algorithms.

2.1. Delay-And-Sum

The original Monostatic Delay-And-Sum (DAS) beamformer is based on the Confocal Microwave Imaging approach [5]. In a Monostatic beamformer, a UWB microwave signal illuminates the breast and microwave energy scattered by potential tumor sites are recorded by the transmitting antenna array element. The DAS beamformer involves time-shifting and summing the backscattered signals from the breast to create a synthetic focus. If a tumor exists at a specific focal point, then the returns from the tumor site will add coherently. Returns from clutter due to variations in tissue types will add incoherently, and therefore will be suppressed. The energy at this synthetic focus is measured and stored, and an energy profile of the breast is created by varying the position of the synthetic focus within the breast.

Consider M Monostatic antennas and let S_n denote the nth backscattered signal, then the energy associated with the focal point $\left(\mathbf{r} = [x, y, z]\right)$ within the breast is defined as:

$$I(\mathbf{r}) = \int_0^{T_{win}} \left[\sum_{n=1}^{M} S_n\Big(t - \tau_n(\mathbf{r})\Big) \right]^2 dt \tag{1}$$

with the nth discrete time delay is described as $\tau_n(\mathbf{r}) = (2d_n(\mathbf{r}))/(vT_s)$, where $d_n(\mathbf{r}) = |\mathbf{r} - \mathbf{r}_n|$ describes the discrete time distance between the nth transmitting antenna $\mathbf{r}_n$ and the focal point $\mathbf{r}$, v describes the average velocity of signal propagation in breast tissue, T_{win} is the window length and T_s is the sampling interval.

Li et al. [6] modified the traditional DAS algorithm in order to compensate for 2D Radial spreading of the UWB pulse. Updating

(Eq. (1)) to:

$$I(\mathbf{r}) = \int_0^{T_{win}} \left[\sum_{n=1}^{M} w_n S_n\Big(t - \tau_n(\mathbf{r})\Big) \right]^2 dt \tag{2}$$

where w_n is the weight component introduced. Furthermore, Fear et al. [7] compensated for radial spreading of the UWB pulse in a 3D system with the application of a weight $(1/(|\mathbf{r} - \mathbf{r}_n|))$ for a planar antenna configuration.

Nilavavan et al. [22] developed the first Multistatic DAS beamformer, where the breast is illuminated by each antenna sequentially and the backscatter energy is recorded at *all* antenna array elements. The increased number of recorded channels reflected outwards via various propagation paths through the tissue acquires more information about scatterers in the breast. M^2 signals are recorded in a Multistatic system but, due to reciprocity, only $M(M+1)/2$ signals are required for the calculation of the energy profile.

2.2. Improved Delay-And-Sum

Klemm et al. [23] atttempted to improve the traditional DAS beamformer by introducing an additional weighting factor, called the Quality Factor (QF), which is a measure of the coherence of UWB backscattering at a particular focal point within the breast. At the focal point ($\mathbf{r}$), energy is collected across a window for each Multistatic signal and stored. The energy from the focal point is then cumulatively summed and plotted against the number of channels used in the process. A second order polynomial is fitted to the normalized energy collection curve ($y = ax^2 + bx + c$) with a assumed to be the Quality Factor. To re-scale the energy collection curve, normalization is carried out by the multiplication of $\left(\frac{1}{1+\sigma_e}\right)$, where σ_e is the standard deviation of the energy of all Multistatic radar signals. The Improved DAS (IDAS) energy equation is represented by:

$$I(\mathbf{r}) = QF(\mathbf{r}) \cdot \int_0^{T_{win}} \left[\sum_{n=1}^{M(M+1)/2} w_n S_n(t - \tau_n(\mathbf{r})) \right]^2 dt \tag{3}$$

2.3. Delay-Multiply-And-Sum

Another variant of the DAS beamformer is the Delay-Multiply-and-Sum (DMAS) beamformer developed by Lim et al. [24]. This algorithm involves signals being time-shifted (as in DAS), multiplied in pairs and

their products summed in order to calculate the energy at a focal point. The energy at ($\mathbf{r}$) can be described as:

$$I(\mathbf{r}) = \int_0^{T_{win}} \left[\sum_{n=1}^{M-1} \sum_{j=(n+1)}^{M} S_n\Big(t - \tau_n(\mathbf{r})\Big) S_j\Big(t - \tau_j(\mathbf{r})\Big) \right]^2 dt \qquad (4)$$

where M describes the number of channels in the system. Lim's approach was tested on a homogenous breast model with dielectric data similar to those used by Fear et al. [7].

3. NUMERICAL MODEL

Finite Difference Time Domain (FDTD) models of the breast were developed to examine the performance of each DI beamformer. Each FDTD model is based on an MRI-derived breast model, taken from the UWCEM breast phantom repository at the University, of Wisconsin, Madison [25]. The intensity of each voxel in the MRI is estimated and mapped to appropriate dielectric properties in the resultant FDTD model [26]. In order to adequately evaluate the beamformers, three breast tissue distributions were considered:

- A Homogenous model, comprising of 3 types of adipose tissue (Figures 1(a) and 1(b)).
- A Normal model, comprising of 3 types of adipose tissue and a single small scattering of medium fibroglandular tissue (Figures 1(c) and 1(d)).
- A Heterogenous model, comprising of all 3 variations of both fibroglandular and adipose tissues (Figures 1(e) and 1(f)).

Dimensions within the 3D region of the breast are described according to each axes. The X axis signifies the depth of the breast, with 0 cm indicating the anterior position. Y and Z represent the span and breadth of the breast respectively, with 0 cm centered at the midpoint of each. A spiculated tumor (to represent a malignant tumor), is artificially introduced into the FDTD model. Tumors are placed in (X(cm), Y(cm), Z(cm)) positions in each simulation, one at $(-8.7, 4.0, 1.0)$ and another at $(-6.2, 2.5, -2.5)$, corresponding to tumor 1 and tumor 2 respectively in Tables 2–4. These tumors are numerically generated from the Gaussian random spheres method [27, 28] to simulate realistic shapes and surface textures. The variation of tumor size is simulated by modifying the inner sphere radius, resulting in tumors of 5 mm, 10 mm and 15 mm diameters.

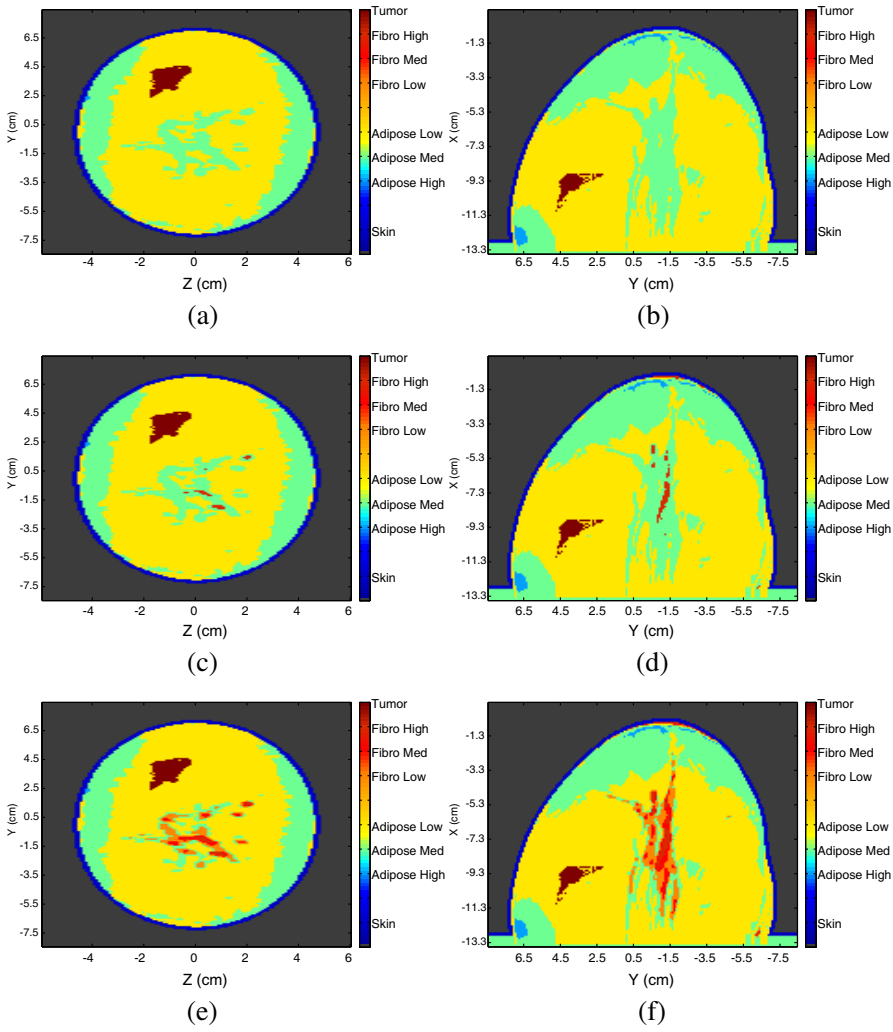

Figure 1. Three breast tissue models with a tumor at $(-8.7, 4.0, 1.0)$. (a) Homogenous model Y-Z slice. (b) Homogenous model X-Y slice. (c) Normal model Y-Z slice. (d) Normal model X-Y slice. (e) Heterogenous model Y-Z slice. (f) Heterogenous model X-Y slice.

The dispersive properties of breast tissue are incorporated into the FDTD model using a single-pole Debye model [29] of the following form:

$$\epsilon_r^*(\omega) = \epsilon_r + \frac{\sigma}{j\omega\epsilon_0} + \frac{\chi_1}{1 + j\omega t_0} \tag{5}$$

The dielectric properties for the variations of adipose and fibroglandular tissue are based on the results described by Zastrow et al. [26]. Skin debye parameters are obtained from published data by Gabriel et al. [30], while debye values representing malignant

Table 1. Debye parameters for the FDTD model.

Tissue	ϵ_r	χ_1	σ	t_0
Skin	15.63	8.2	0.82	12.6
Tumor	7	47	0.15	7
Adipose (Low)	2.85	1.10	0.025	13
Fibroglandular (Low)	12.85	24.64	0.251	13
Adipose (Medium)	3.12	1.59	0.050	13
Fibroglandular (Medium)	13.81	35.55	0.738	13
Adipose (High)	3.98	3.54	0.080	13
Fibroglandular (High)	14.28	40.52	0.638	13

Table 2. Homogenous tissue distribution metric results.

		SMR(dB)				**SCR(dB)**			
Tumor	**Radius(mm)**	**DASM**	**DAS**	**DMAS**	**IDAS**	**DASM**	**DAS**	**DMAS**	**IDAS**
1	2.5	8.74	14.67	18.77	17.02	0.45	11.88	22.84	18.49
	5.0	10.38	12.88	16.88	13.90	4.41	10.48	18.10	11.93
	7.5	12.19	11.81	15.53	13.01	5.54	8.47	17.13	9.31
2	2.5	9.12	14.73	18.27	15.94	2.43	11.78	17.64	15.21
	5.0	9.73	13.24	16.94	16.20	2.95	9.90	18.50	13.90
	7.5	10.56	11.85	15.40	14.48	4.89	4.24	13.62	10.39
Average		**10.12**	**13.19**	**16.97**	**15.09**	**3.44**	**9.46**	**17.97**	**13.20**

Table 3. Normal tissue distribution metric results.

		SMR(dB)				**SCR(dB)**			
Tumor	**Radius(mm)**	**DASM**	**DAS**	**DMAS**	**IDAS**	**DASM**	**DAS**	**DMAS**	**IDAS**
1	2.5	6.38	9.81	12.88	6.38	–1.27	–1.98	–3.85	–7.31
	5.0	8.45	11.91	16.66	13.88	0.65	5.14	10.82	11.55
	7.5	8.80	11.00	15.19	12.55	1.87	5.55	11.75	6.29
2	2.5	5.72	7.51	6.20	0.90	–2.28	–5.87	–12.25	–14.45
	5.0	7.95	11.08	15.39	10.30	0.57	1.54	2.74	–1.39
	7.5	7.51	10.02	14.02	9.05	–0.07	0.91	1.97	–2.67
Average		**7.47**	**10.22**	**13.39**	**8.84**	**–0.09**	**0.88**	**1.86**	**–1.33**

Table 4. Heterogenous tissue distribution metric results.

		SMR(dB)				SCR(dB)			
Tumor	**Radius(mm)**	**DASM**	**DAS**	**DMAS**	**IDAS**	**DASM**	**DAS**	**DMAS**	**IDAS**
1	2.5	2.78	–4.71	–14.24	–18.95	–5.21	–12.23	–24.90	–28.76
	5.0	4.99	2.19	0.19	–9.82	–3.21	–4.75	–10.01	–19.66
	7.5	5.05	1.92	–0.15	–7.68	–3.03	–4.88	–10.39	–17.75
2	2.5	0.98	–1.96	–8.76	–13.58	–6.30	–9.58	–19.87	–24.88
	5.0	2.81	3.55	2.99	–7.55	–4.41	–3.48	–7.73	–18.86
	7.5	2.20	2.07	0.66	–8.00	–5.08	–4.74	–9.70	–19.19
Average		**3.14**	**0.51**	**–3.22**	**–10.93**	**–4.54**	**–6.61**	**–13.77**	**–21.52**

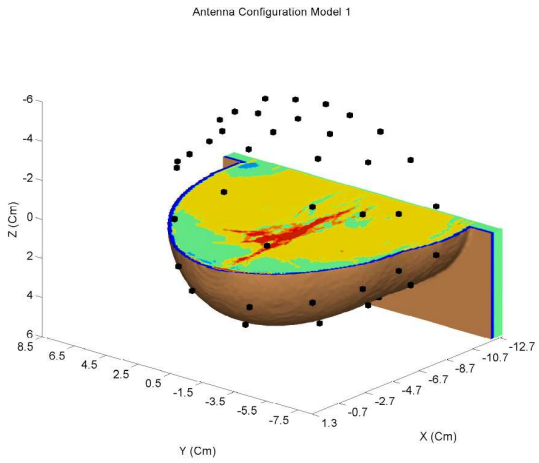

Figure 2. Antenna configuration.

tissue are taken from Bond et al. [8]. The breast is surrounded by a synthetic material matching the dielectric properties of skin. All single pole debye parameters are described in Table 1. The overall FDTD grid size is approximately 28.8 million cubic cells, the grid resolution is $(1\,\text{mm}(dx) \times 1\,\text{mm}(dy) \times 1\,\text{mm}(dz))$ and the time step dt is defined as 0.833 ps $(dx/2c)$, where c is the speed of light in a vacuum. The FDTD grid is terminated on each side by a 12 layer UPML [31] in order to minimize edge reflections. In total, 18 FDTD simulations were carried out, based on three distributions of tissue, the two tumor locations and the three different tumor sizes.

A cylindrical antenna array [7], consisting of half-wavelength dipole antennas, is placed around the breast. Fifty three antennas

are arranged on five rings, as illustrated in Figure 2. The antenna array elements are placed on the skin, with a uniform spacing of 22 mm between each ring along the X axis. The UWB input pulse is a 120 ps differentiated Gaussian pulse, with a center frequency of 7.5 GHz and a -3 dB bandwidth of 9 GHz. The wavelength of the waveguide in breast tissue is approximately 4 cm, dictating the length of the dipole at 2 cm. An ideal artifact removal algorithm is applied to the backscattered signals to remove the input signal and any reflection from the skinbreast interface, as previously used by Xie et al. [10]. Prior to any signal processing, all FDTD signals are downsampled from 1200 GHz to 50 GHz.

4. METRICS

The following metrics are used in order to evaluate each beamformers performance:

- Signal to Mean ratio (SMR)
- Signal to Clutter ratio (SCR)

The Signal to Mean ratio (SMR) describes the ratio of the tumor response to the average energy response of all tissue types within the breast. The Signal to Clutter ratio (SCR) is defined as the ratio of the tumor response to the maximum clutter response in the same breast. This response is assumed to be the peak energy outside the area defined by twice the the physical extent of the tumor, or Full Width Half Maximum (FWHM) [7]. The FWHM itself is defined as the distance from the tumor response to where the tumor response energy drops by half.

5. RESULTS

Resulting images from each beamformer are shown in Figures 3–6 as a Y-Z and associated X-Y cross-sectional slice (the tumor location is indicated by a pink circle for clarification in the case of the Normal and Heterogenous tissue models). Furthermore, the corresponding performance metrics (SMR and SCR) are shown in Tables 2–4. Each table corresponds to a particular level of dielectric heterogeneity.

In the Homogenous model, both DMAS and IDAS significantly outperform the Multistatic and Monostatic DAS beamformer as shown in Table 2. DMAS and IDAS have an average SMR results of 16.97 dB and 15.09 dB respectively compared to 13.19 dB and 10.12 dB for Multistatic and Monostatic DAS respectively. On average, the SCR values for the IDAS and DMAS beamformers are respectively:

3.74 dB and 8.51 dB greater than for the Multistatic DAS. The weakest algorithm is the Monostatic DAS with an average SMR of 10.12 dB and an SCR of 3.44.

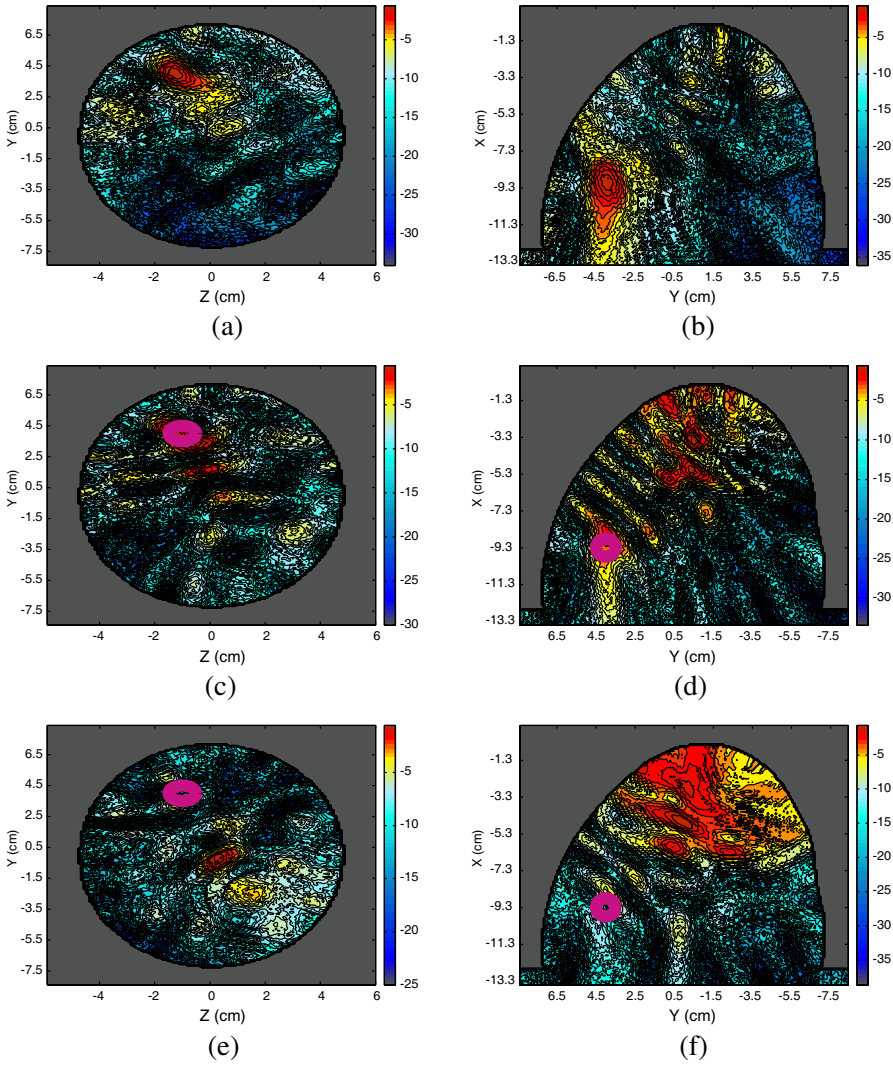

Figure 3. DAS Monostatic beamformed images for a tumor located at $(-8.7, 4.0, 1.0)$. (a) Homogenous model Y-Z slice. (b) Homogenous model X-Y slice. (c) Normal model Y-Z slice. (d) Normal model X-Y slice. (e) Heterogenous model Y-Z slice. (f) Heterogenous model X-Y slice.

Examining these results in this simple breast model, the beamformers assumed propagation model and the actual propagation channel are very similar, and therefore coherent addition of the

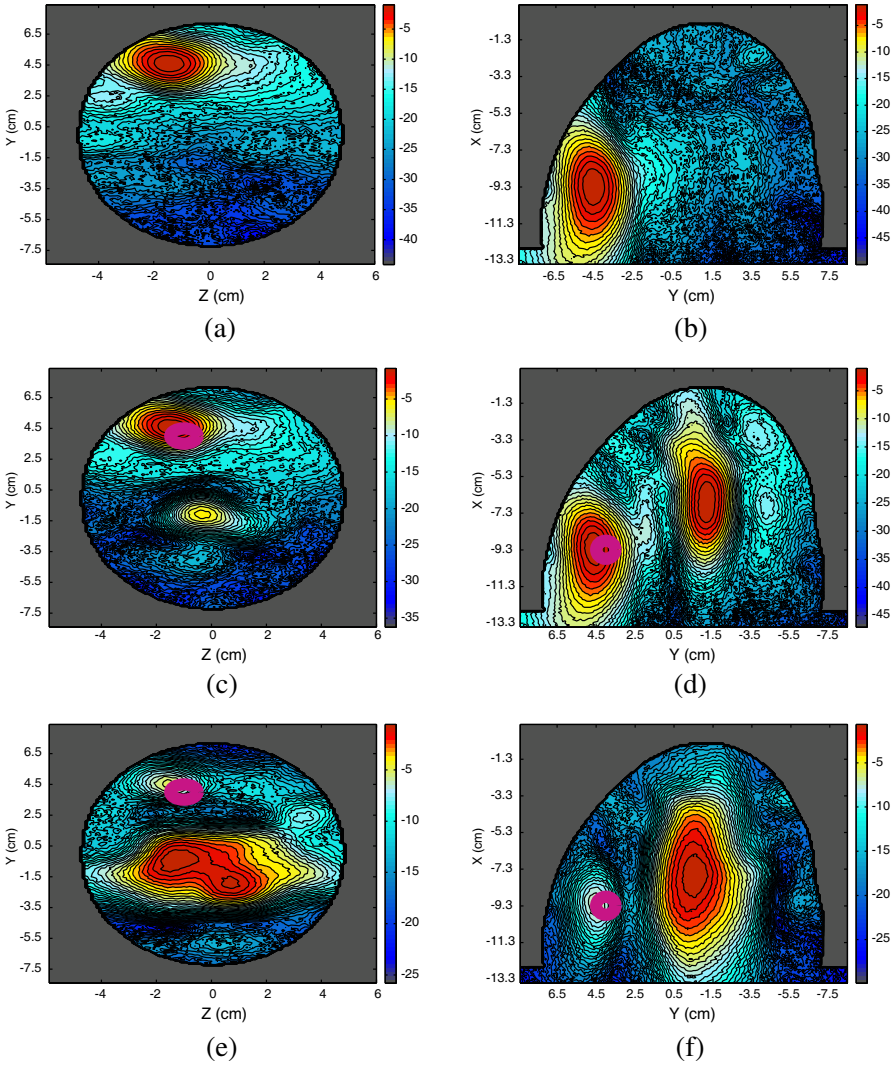

Figure 4. DAS Multistatic beamformed images for a tumor located at $(-8.7, 4.0, 1.0)$. (a) Homogenous model Y-Z slice. (b) Homogenous model X-Y slice. (c) Normal model Y-Z slice. (d) Normal model X-Y slice. (e) Heterogenous model Y-Z slice. (f) Heterogenous model X-Y slice.

backscattered responses is relatively simple. Since the DMAS and IDAS beamformer reward coherency, they tend to offer considerable improvement over the DAS beamformer in relatively homogeneous breast models.

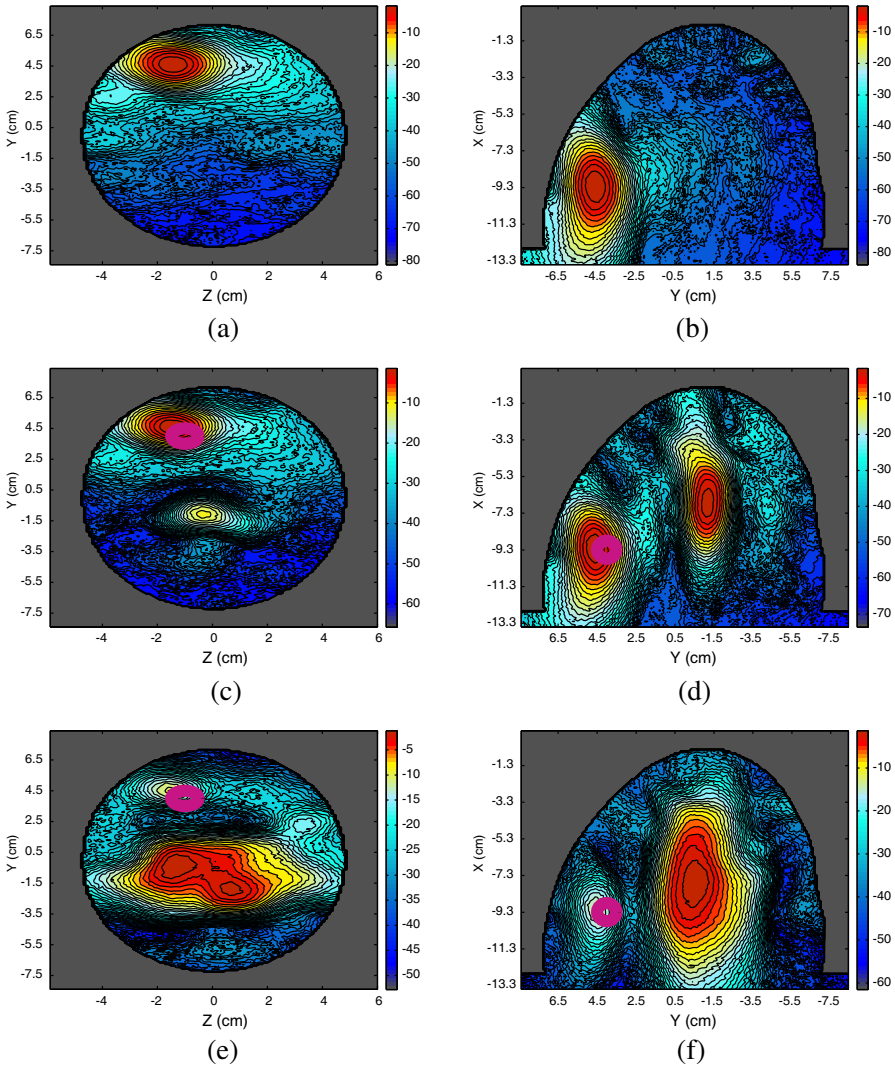

Figure 5. DMAS beamformed images for a tumor located at $(-8.7, 4.0, 1.0)$. (a) Homogenous model Y-Z slice. (b) Homogenous model X-Y slice. (c) Normal model Y-Z slice. (d) Normal model X-Y slice. (e) Heterogenous model Y-Z slice. (f) Heterogenous model X-Y slice.

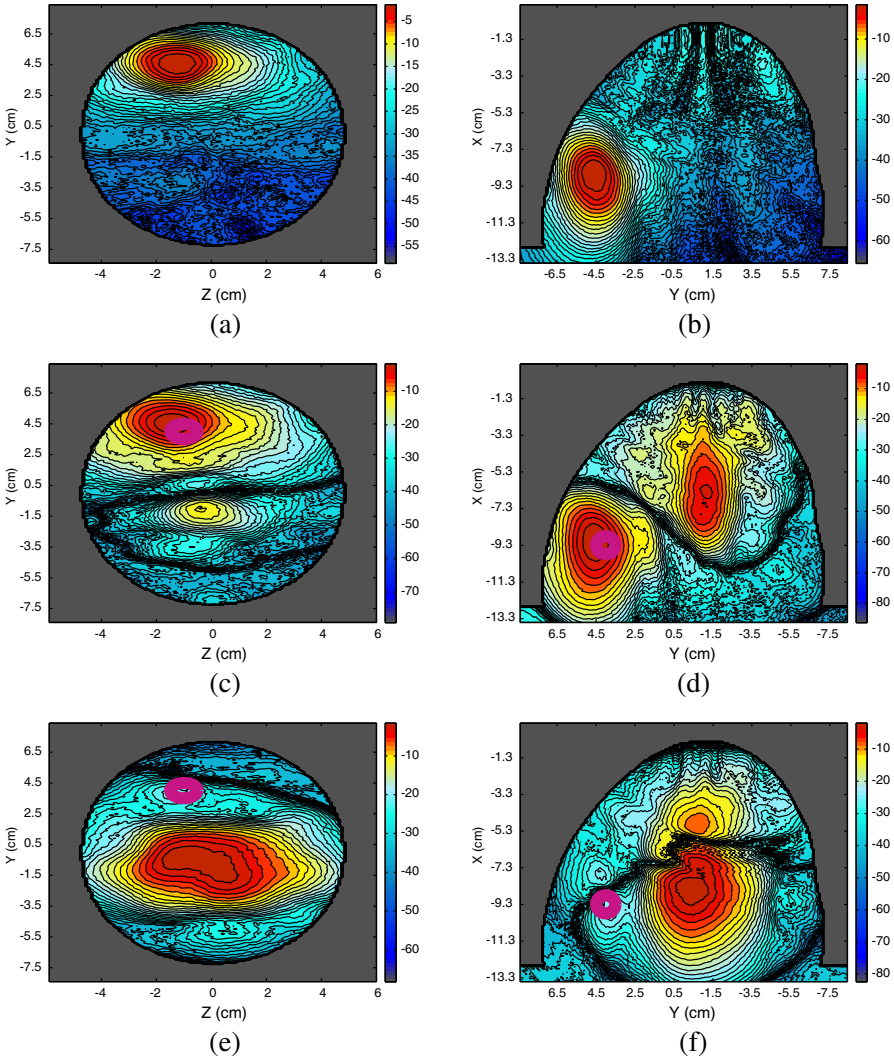

Figure 6. I-DAS beamformed images for a tumor located at $(-8.7, 4.0, 1.0)$. (a) Homogenous model Y-Z slice. (b) Homogenous model X-Y slice. (c) Normal model Y-Z slice. (d) Normal model X-Y slice. (e) Heterogenous model Y-Z slice. (f) Heterogenous model X-Y slice.

In the Normal breast model, the performance of the IDAS beamformer is particularly reduced, with an average SMR of 8.84 dB and an average SCR of -1.33 dB (compared to 15.09 dB and 13.20 dB for the homogeneous model). DMAS outperforms Multistatic DAS by

an average of 3.19 dB and 0.98 dB for SMR and SCR across all tumors. Monostatic DAS offers a better average SCR than IDAS of 1.24 dB, but still performs poorly compared the Multistatic DAS beamformer which gives an improvement of 2.75 dB and 0.97 dB for SMR and SCR respectively over it's Monostatic counterpart.

The performance of all beamforming algorithms degrade with the presence of a small region of fibroglandular tissue compared to the Homogenous model, as shown in Table 3. The breast can no-longer be considered homogenous, and the contrast between the assumed and actual propagation channel affects the performance of the each beamformer. IDAS performance degrades significantly since the beamformer is based on the principle of weighting voxels where coherent addition occurs, and coherent addition is much more difficult with increasing levels of dielectric heterogeneity.

Based on the results in Table 4, the DAS algorithm is the most effective beamformer when applied to the dielectrically heterogenous breast, with Monostatic DAS achieving an average SCR of −4.54 dB and an average SMR of 3.14 dB. Multistatic DAS offers an improvement in SMR of 3.73 dB and 11.44 dB over DMAS and IDAS respectively. Average SCR results for Multistatic DAS (−6.61 dB) are 14.91 dB and 7.16 dB greater than the average IDAS and DMAS SCR results respectively.

Visibly discerning between tumor and non-tumor locations in the Heterogenous model becomes very difficult, with the peak energy response often occurring within the region of fibroglandular tissue. Results for DMAS and IDAS are markedly reduced when compared to the normal and homogenous breast results illustrating their dependence on a dielectrically homogeneous propagation channel.

6. CONCLUSIONS

In this paper, four DI UWB radar breast imaging systems are evaluated. Beamforming algorithms are tested on signals taken from a number of realistic and dielectrically accurate electromagnetic breast models. For test purposes 18 3D FDTD models were created, with a tumor placed at two different locations within the breast. The DAS, DMAS and IDAS beamforming algorithms were examined using two metrics: SCR and SMR.

With a varying contrast in dielectric breast profiles in the breast, the performance of each DI approach degrades significantly. All DI beamformers assume a homogenous dielectric breast structure for the calculation of the propagation delay of the UWB pulse through breast tissue. In general, the shortcomings of this assumption are evident with

each beamformer once the level of dielectric heterogeneity increases within the breast, leading to inaccuracies between the assumed and actual channel model. The multiplication of time aligned peak responses become distorted in the case of DMAS and the cumulative energy summation carried out by the IDAS algorithm is skewed.

DAS was found to be the most robust beamformer in difficult imaging scenarios with Monostatic DAS offering superior results in a heterogenetically dense breast. The distortion has less effect on the time aligned summation of the tumor response than the multiplication or energy summation employed by DMAS and IDAS respectively.

Future work will involve testing the other approaches to the microwave imaging problem space, particularly investigating the performance of Data-Adaptive beamforming algorithms on breast models with varying levels of dielectric heterogeneity.

REFERENCES

1. Society, A. C., "Cancer facts and figures 2009," Tech. Rep., American Cancer Society, Atlanta, 2009.
2. Ferlay, J., P. Autier, M. Boniol, M. Heanue, M. Colombet, and P. Boyle, "Estimates of the cancer incidence and mortality in europe in 2006," *Annals of Oncology*, Vol. 18, 581–592, 2007.
3. Nass, S. L., I. C. Henderson, and J. C. Lashof, *Mammography and Beyond: Developing Technologies for the Early Detection of Breast Cancer*, National Academy Press, 2001.
4. Huynh, P. H., A. M. Jarolimek, and S. Daye, "The false-negative mammogram," *RadioGraphics*, Vol. 18, 1137–1154, 1998.
5. Hagness, S. C., A. Taflove, and J. E. Bridges, "Two-dimensional fdtd analysis of a pulsed microwave confocal system for breast cancer detection: Fixed focus and antenna array sensors," *IEEE Transactions on Biomedical Engineering*, Vol. 45, 1470–1479, 1998.
6. Li, X. and S. C. Hagness, "A confocal microwave imaging algorithm for breast cancer detection," *IEEE Microwave and Wireless Communications Letters*, Vol. 11, 130–132, 2001.
7. Fear, E. C., X. Li, S. C. Hagness, and M. A. Stuchly, "Confocal microwave imaging for breast cancer detection: Localization of tumors in three dimensions," *IEEE Transactions on Biomedical Engineering*, Vol. 47, 812–812, 2002.
8. Bond, E. J., X. Li, S. C. Hagness, and B. D. V. Veen, "Microwave imaging via space-time beamforming for early detection of breast

cancer," *IEEE Transactions on Antennas and Propagation*, 1690–1705, 2003.

9. Kosmas, P. and C. M. Rappaport, "Time reversal with the fdtd method for microwave breast cancer detection," Vol. 53, No. 7, 2317–2323, 2005.
10. Xie, Y., B. Guo, L. Xu, J. Li, and P. Stoica, "Multi-static adaptive microwave imaging for early breast cancer detection," *IEEE Transactions on Biomedical Engineering*, Vol. 53, 1647–1657, 2006.
11. Meaney, P. M., M. W. Fanning, D. Li, S. P. Poplack, and K. D. Paulsen, "A clinical prototype for active microwave imaging of the breast," IEEE *Trans. Microwave Theory Tech.*, Vol. 48, No. 11, 1841–1853, Nov. 2000.
12. Meaney, P. M., M. W. Fanning, T. Raynolds, C. J. Fox, Q. Fang, C. A. Kogel, S. P. Poplack, and K. D. Paulsen, "Initial clinical experience with microwave breast imaging in women with normal mammography," *IEEE Trans. Microwave Theory Tech.*, Vol. 48, No. 11, 1841–1853, Nov. 2000.
13. Kruger, R. A., K. D. Miller, H. E. Reynolds, W. L. Kiser, D. R. Reinecke, and G. A. Kruger, "Breast cancer in vivo: Contrast enhancement with thermoacoustic ct at 434 MHz — Feasibility study," *Radiology*, Vol. 216, No. 1, 279–283, 2000.
14. Zhao, M., J. D. Shea, S. C. Hagness, D. W. van der Weide, B. D. V. Veen, and T. Varghese, "Numerical study of microwave scattering in breast tissue via coupled dielectric and elastic contrasts," *IEEE Antennas and Wireless Propagation Letters*, Vol. 7, 247–250, 2008.
15. O'Halloran, M., E. Jones, and M. Glavin, "Quasi-multistatic mist beamforming for the early detection of breast cancer," *IEEE Transactions on Biomedical Engineering*, Vol. 57, No. 4, 830–840, Apr. 2010.
16. O'Halloran, M., M. Glavin, and E. Jones, "Effects of fibroglandular tissue distribution on data-independent beamforming algorithms," *Progress In Electromagnetics Research*, Vol. 97, 141–158, 2009.
17. Jossinet, J., "The impedivity of freshly excised human breast tissue," *Physiol. Meas.*, Vol. 19, 61–75, 1998.
18. Gabriel, S., R. W. Lau, and C. Gabriel, "The dielectric properties of biological tissues: III. Parametric models for the dielectric spectrum of tissues," *Physics in Medicine and Biology*, Vol. 41, 2271–2293, 1996.

19. Lazebnik, M., L. McCartney, D. Popovic, C. B. Watkins, M. J. Lindstrom, J. Harter, S. Sewall, A. Magliocco, J. H. Booske, M. Okoniewski, and S. C. Hagness, "A large-scale study of the ultrawideband microwave dielectric properties of normal breast tissue obtained from reduction surgeries," *Physics in Medicine and Biology*, Vol. 52, 2637–2656, 2007.
20. Lazebnik, M., D. Popovic, L. McCartney, C. B. Watkins, M. J. Lindstrom, J. Harter, S. Sewall, T. Ogilvie, A. Magliocco, T. M. Breslin, W. Temple, D. Mew, J. H. Booske, M. Okoniewski, and S. C. Hagness, "A large-scale study of the ultrawideband microwave dielectric properties of normal, benign and malignant breast tissues obtained from cancer surgeries," *Physics in Medicine and Biology*, Vol. 52, 6093–6115, 2007.
21. Conceicao, R., M. O'Halloran, M. Glavin, and E. Jones, "Comparison of planar and circular antenna configurations for breast cancer detection using microwave imaging," *Progress In Electromagnetics Research*, Vol. 99, 1–19, 2009.
22. Nilavalan, R., S. C. Hagness, and B. D. V. Veen, "Numerical investigation of breast tumour detection using multi-static radar," *IEE Electronic Letters*, Vol. 39, No. 25, 1787–1789, Dec. 2003.
23. Klemm, M., I. Craddock, J. Leendertz, A. Preece, and R. Benjamin, "Improved delay-and-sum beamforming algorithm for breast cancer detection," *International Journal of Antennas and Propogation*, Vol. 2008, 9, 2008.
24. Lim, H. B., N. T. T. Nhung, E.-P. Li, and N. D. Thang, "Confocal microwave imaging for breast cancer detection: Delay-multiplyand sum image reconstruction algorithm," *IEEE Transactions on Biomedical Engineering*, Vol. 55, No. 6, 1697–1704, Jun. 2008.
25. Zastrow, E., S. K. Davis, M. Lazebnik, F. Kelcz, B. D. V. Veen, and S. C. Hagness, "Database of 3d grid-based numerical breast phantoms for use in computational electromagnetics simulations," Department of Electrical and Computer Engineering University of Wisconsin-Madison, [Online], 2008, Available: http://uwcem.ece.wisc.edu/home.htm.
26. Zastrow, E., S. K. Davis, M. Lazebnik, F. Kelcz, B. D. V. Veen, and S. Hagness, "Development of anatomically realistic numerical breast phantoms with accurate dielectric properties for modeling microwave interactions with the human breast," *IEEE Transactions on Biomedical Engineering*, Vol. 55, No. 12, 2792–2800, Dec. 2008.
27. Davis, S. K., B. D. V. Veen, S. C. Hagness, and F. Kelcz, "Breast tumor characterization based on ultrawideband backscatter,"

IEEE Transactions on Biomedical Engineering, Vol. 55, No. 1, 237–246, 2008.

28. Muinonen, K., "Introducing the gaussian shape hypothesis for asteroids and comets," *Astronomy and Astrophysics*, Vol. 332, 1087–1098, 1998.
29. Okoniewski, M., M. Mrozowski, and M. A. Stuchly, "Simple treatment of multi-term dispersion in fdtd," *IEEE Microwave and Guided Wave Letters*, Vol. 7, 121–123, 1997.
30. Gabriel, C., S. Gabriel, and E. Corthout, "The dielectric properties of biological tissues: I. literature survey," *Phys. Med. Biol.*, Vol. 41, No. 11, 2231–2249, Nov. 1996.
31. Berenger, J. P., "A perfectly matched layer for the absorption of electromagnetic waves," *Journal of Computational Physics*, Vol. 114, 185–200, 1994.